Journal of Computational Physics **153,** 378–402 (1999)
Article ID jcph.1999.6282, available online at http://www.idealibrary.com on IDEAL®

A Direct Spectral Method for Determination of Flows over Corrugated Boundaries

J. Szumbarski and J. M. Floryan

Department of Mechanical and Materials Engineering, The University of Western Ontario, London, Ontario, N6A 5B9, Canada

Received March 29, 1999

A completely spectral algorithm for analysis of flows over corrugated boundaries is proposed. The algorithm treats the flow problem as an internal rather then a boundary value problem, where the flow conditions are specified along a line in the interior of the computational domain. The method eliminates the need for a coordinate generation and/or premapping required for regularization of the computational domain in standard implementations of spectral discretizations. Various tests confirm the spectral accuracy of the algorithm. © 1999 Academic Press

1. INTRODUCTION

Flows over corrugated boundaries are of interest in many applications. Good examples are the use of grooved surfaces in reduction of skin friction drag [8, 9], high-efficiency membrane oxygenerators [11], analysis of the process of wave growth under the action of wind [4], and analysis of the laminar–turbulent transition process in flows over rough surfaces [5], among others. The main difficulty in simulation of such flows is associated with treatment of boundary conditions on a geometrically irregular boundary.

There are two main approaches available in the literature. The first one, which we shall refer to as the domain perturbation, involves transfer of boundary conditions to a certain mean location, resulting in a regular computational domain. The accuracy of the domain perturbation depends on the type of boundary condition transfer procedure. The applicability of the first-order procedure, which is well described in [7] in the context of flow over a rough leading edge, is limited to situations where the boundary corrugations produce flow modifications that can be described by a linear theory.

The second approach involves construction of a coordinate system where one of the coordinate lines overlaps with the corrugated boundary. Sobey [11] analyzed furrowed periodic channels and used an analytical mapping resulting in a non-orthogonal reference system. Caponi *et al.* [4] employed an orthogonal transformation expressed in terms of an infinite series in their analysis of boundary layers over wavy surfaces. Benjamin [2]

0021-9991/99 $30.00

considered a coordinate system based on streamlines of an inviscid flow over a wavy wall in his analysis of shear flows over wavy walls. Balasubranian and Orszag [1] employed numerically generated conformal mapping in their simulations of flows over wavy walls.

Other possible approaches include a full range of numerical coordinate generation procedures [12], unstructured domain decomposition methods [10], and numerical conformal mapping specifically tuned to periodic geometries [6]. The last two methodologies have been extended to higher-order accuracy [6, 10]. Lack of spectrally accurate grid generation techniques, however, limits the development of spectrally accurate algorithms. Nevertheless, one may combine any grid generation technique with the spectral discretization of the field equations as done, for example, in [1].

The main goal of the present analysis is the development of a fully spectral algorithm capable of simulating flows over corrugated boundaries. This is achieved by posing the numerical problem as an internal problem rather than a boundary value problem. The computational domain is larger than the flow domain and completely surrounds it. The flow boundary conditions are imposed along a line that weaves through the interior of the computational domain; i.e., the boundaries of the flow and computational domains do not necessarily coincide.

This paper is organized as follows. Section 2 describes a model problem, which is used to illustrate the algorithm. Section 3 provides a description of the algorithm. Section 4 discusses results of various numerical tests. Section 5 provides a short summary of the main conclusions.

2. PROBLEM FORMULATION

We shall describe our algorithm in the context of a convenient model problem. The selected model problem consists of a viscous flow driven by a pressure gradient through a channel with corrugated walls.

2.1. *Reference Flow*

Consider plane Poiseuille flow confined between flat rigid walls at $y = \pm 1$ and extending to infinity in the x-direction (Fig. 1a). The fluid motion is described by the velocity and pressure fields

$$\bar{V}_0(\bar{x}) = [u_0(x, y), v_0(x, y)] = [u_0(y), 0] = [1 - y^2, 0], \qquad p_0(\bar{x}) = -2x/\mathrm{Re}, \quad (2.1)$$

where the fluid is directed towards the positive x-axis, and the Reynolds number Re is based on the half-channel height and the maximum x-velocity. This flow is driven by a constant negative pressure gradient.

2.2. *Flow in a Corrugated Channel*

Consider the upper and lower walls to have arbitrary shapes described by $y_U(x)$ and $y_L(x)$ (Fig. 1b), respectively, and characterized by a certain periodicity with wavelength $\lambda_x = 2\pi/\alpha$. The shape of the walls can be expressed in terms of Fourier series in the form

$$y_L(x) = \sum_{n=-\infty}^{n=\infty} (A_n)_L e^{in\alpha x}, \qquad y_U(x) = \sum_{n=-\infty}^{n=\infty} (A_n)_U e^{in\alpha x}, \quad (2.2)$$

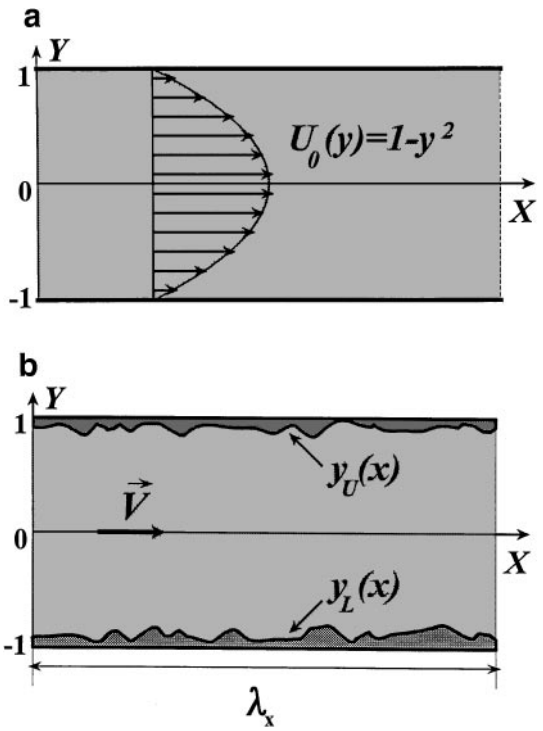

FIG. 1. Sketch of the flow domain. (a) Straight (reference) channel. (b) Channel with corrugated walls. The flow domain (dotted area) forms a subset of the rectangular domain.

where $(A_0)_L = -1 + H_L$, $(A_0)_U = 1 - H_U$, and $(A_n)_L = (A_{-n})_L^\star$ and $(A_n)_U = (A_{-n})_U^\star$ in order for $y_U(x)$ and $y_L(x)$ to be real, and the star denotes the complex conjugate. The subscript L refers to the bottom wall, while the subscript U refers to the upper wall of the channel. In addition, it is assumed that

$$\min_{0\le x\le 2\pi/\alpha} y_L(x) \ge -1, \qquad \max_{0\le x\le 2\pi/\alpha} y_U(x) \le 1,$$

i.e., the flow domain is bounded by $-\infty < x < \infty$, $-1 \le y \le 1$ (see Fig. 1b). The flow in the channel can be represented as

$$\begin{aligned}\bar{V}(\bar{x}) &= [u(x,y), v(x,y)] = \bar{V}_0(\bar{x}) + \bar{V}_1(\bar{x}) \\ &= [u_0(y), 0] + [u_1(x,y), v_1(x,y)], \qquad p(\bar{x}) = p_0(\bar{x}) + p_1(\bar{x}),\end{aligned} \tag{2.3}$$

where $\bar{V}_1$ and p_1 are the velocity and pressure modifications due to the presence of wall corrugations. Substitution of the above representation of the flow quantities into the Navier–Stokes and continuity equations results in the following form of the governing equations,

$$\begin{aligned} u_0\partial_x u_1 + u_1\partial_x u_1 + v_1 Du_0 + v_1\partial_y u_1 &= -\partial_x p_1 + \frac{1}{\mathrm{Re}}(\partial_{xx}u_1 + \partial_{yy}u_1), \\ u_0\partial_x v_1 + u_1\partial_x v_1 + v_1\partial_y v_1 &= -\partial_y p_1 + \frac{1}{\mathrm{Re}}(\partial_{xx}v_1 + \partial_{yy}v_1), \quad \partial_x u_1 + \partial_y v_1 = 0, \end{aligned} \tag{2.4}$$

where the symbol ∂ denotes partial differentiation, subscripts x and y denote the arguments of partial differentiations, and $D = d/dy$. Introduction of the stream function defined as

$$u_1 = \partial_y \Psi, \qquad v_1 = -\partial_x \Psi,$$

and elimination of pressure permits expression of the field equations (2.4) in the form

$$(u_0 \partial_x + \partial_y \Psi \partial_x - \partial_x \Psi \partial_y)\Delta \Psi - D^2 u_0 \partial_x \Psi = \frac{1}{\mathrm{Re}} \Delta^2 \Psi, \tag{2.5}$$

where Δ denotes the Laplace operator. Since u_1 and v_1 are periodic in x with the period $\lambda_x = 2\pi/\alpha$, the stream function can be represented as

$$\Psi(x, y) = \sum_{n=-\infty}^{n=+\infty} \Phi_n(y) e^{in\alpha x}, \tag{2.6}$$

where $\Phi_n = \Phi^{\star}_{-n}$. In general, one cannot exclude the possibility that subharmonics exist in the velocity field. Their presence, however, can be accounted for by a simple change of indices in (2.6). No subharmonics were found for parameter ranges used in the numerical tests (see discussion in Section 4).

The functions Φ_n, $n \geq 0$, in (2.6) are governed by a nonlinear system of ordinary differential equations in the form

$$\begin{aligned} &\left[D_n^2 - in\alpha \,\mathrm{Re}\left(u_0 D_n - D^2 u_0\right)\right]\Phi_n \\ &\quad - i\alpha \,\mathrm{Re} \sum_{k=-\infty}^{k=+\infty} [k D\Phi_{n-k} D_k \Phi_k - (n-k)\Phi_{n-k} D_k D\Phi_k] = 0, \end{aligned} \tag{2.7}$$

where $D_n = D^2 - n^2\alpha^2$. Equation (2.7) has been obtained by substituting (2.6) into (2.5) and separating Fourier components.

The boundary conditions at the channel walls are expressed in the form

$$\begin{aligned} u_0(y_L(x)) + u_1(x, y_L(x)) = 0 \quad &\text{and} \quad v_1(x, y_L(x)) = 0 \quad \text{at } y = y_L(x), \\ u_0(y_U(x)) + u_1(x, y_U(x)) = 0 \quad &\text{and} \quad v_1(x, y_U(x)) = 0 \quad \text{at } y = y_U(x). \end{aligned} \tag{2.8}$$

The numerical implementation of these conditions is discussed in the next section.

Problem formulation is closed by specifying two additional conditions. The first condition is associated with the introduction of the stream function and can be selected arbitrarily without affecting the generality of the formulation. The second condition arises due to the fact that an x-periodic velocity field may be associated with a pressure field that has a component linear in x. For simplification of physical interpretation of the results, this condition can be cast in terms of the volume flux, in terms of the pressure gradient, or in terms of any combination of both of them. The condition based on the volume flux has been selected for presentation of the algorithm due to its simplicity. This condition involves only kinematic characteristics of the flow and can be cast as

$$\Psi_0(y_L(x)) + \Psi(x, y_L(x)) = T, \qquad \Psi_0(y_U(x)) + \Psi(x, y_U(x)) = T + Q_0, \tag{2.9}$$

where Ψ_0 denotes the stream function of the Poiseuille flow ($\Psi_0(-1) = 0$), Q_0 stands for the (specified) volume flux, and T denotes an arbitrary constant. In all calculations

presented, the volume flux in the corrugated channel has been set as $Q_0 = \frac{4}{3}$, i.e., it is the same as the volume flux in the straight channel.

3. NUMERICAL DISCRETIZATION METHOD

The problem to be solved numerically consists of an infinite system of nonlinear ordinary differential equations (2.7) subject to boundary conditions (2.8)–(2.9). This section is devoted primarily to describing the numerical discretization of the above problem.

As a first step, the representation of the stream function of the flow modifications Ψ is truncated to M leading Fourier modes, i.e.,

$$\Psi(x, y) \approx \sum_{n=-M}^{n=M} \Phi_n(y) e^{in\alpha x}. \tag{3.1}$$

The corresponding, finite dimensional system of the ordinary differential equations for the functions Φ_n, $n = 0, 1, \ldots, M$, can easily be written on the basis of Eq. (2.7). This system can be discretized with spectral accuracy by introducing Chebyshev representations of the unknown function Φ_n,

$$\Phi_n(y) = \sum_{j=0}^{j=\infty} G_j^n T_j(y) \approx \sum_{j=0}^{j=K} G_j^n T_j(y), \tag{3.2}$$

where T_j denotes the Chebyshev polynomial of the jth order and G_j^n stands for the unknown expansion coefficient. The Chebyshev representations of the required derivatives $D^l\Phi$ (with l up to $l = 4$) can be determined using a recursive algorithm described on p. 62 in [3].

The nth equation of our system can be written in a general form as

$$\Xi_n(\Phi_0, \Phi_1, \ldots, \Phi_M) = 0 \qquad \text{for } n = 0, \ldots, M. \tag{3.3}$$

The substitution of the Chebyshev expansions (3.2) and their derivatives into (3.3) gives the residual function

$$R_n = \Xi_n\left(\sum_{j=0}^{j=K} G_j^0 T_j,\ \sum_{j=0}^{j=K} G_j^1 T_j, \ldots,\ \sum_{j=0}^{j=K} G_j^M T_j\right), \qquad n = 0, \ldots, M. \tag{3.4}$$

The problem is converted to an algebraic, nonlinear system by imposing the orthogonality conditions

$$\langle R_n, T_j\rangle_\omega = 0, \qquad j = 0, \ldots, K-4, \quad n = 0, \ldots, M. \tag{3.5}$$

The inner product used in (3.5) is defined as

$$\langle f, g\rangle_\omega := \int_{-1}^{1} f(x)g(x)\omega(x)\,dx, \qquad \omega(x) = (1-x^2)^{-1/2}.$$

Since the orthogonality properties of Chebyshev polynomials

$$\langle T_m, T_n\rangle_\omega = 0 \quad \text{for } m \neq n \qquad \text{and} \qquad \langle T_m, T_m\rangle_\omega = \begin{cases} \pi & \text{for } m = 0 \\ \pi/2 & \text{for } m > 0 \end{cases}$$

take place, conditions (3.5) ensure a spectral rate of convergence with respect to the truncation threshold K in the expansions (3.2) provided that the solution being approximated is smooth.

The discretization method described above can be viewed as a variant of the Chebyshev-tau technique. The reader should note that the projection is carried out onto the linear subspace spanned by the Chebyshev polynomials with the order of up to K-4. The additional equations required to close the system are due to flow boundary conditions (2.8) and volume flux conditions (2.9).

Numerical treatment of flow boundary conditions, which are to be enforced along the lines $y_L(x)$ and $y_U(x)$, poses a challenge and, at the same time, represents unique features of the proposed method. To explain the current approach to the boundary conditions we evaluate velocity components $u_l(x) = u(x,\ f(x))$ and $v_l(x) = v(x,\ f(x))$ along an arbitrary line $l := \{(x, y) : y = f(x)\}$, such that the function f is periodic with the period $\lambda_x = 2\pi/\alpha$, and $|f(x)| \leq 1$. This function can be expressed, without loss of generality, as a Fourier expansion in the form

$$f(x) = \sum_{n=-N_A}^{n=N_A} A_n e^{in\alpha x}. \tag{3.6}$$

The number of terms N_A is arbitrary, however; only expansions with a finite number of terms can be handled in the actual computations. Both velocity components u_l and v_l are x-periodic functions, with the same period λ_x , and thus can be expressed in terms of Fourier series as

$$u_l(x) \equiv u(x,\ f(x)) = \sum_{n=-N_U}^{n=N_U} U_n e^{in\alpha x}, \qquad v_l(x) \equiv v(x,\ f(x)) = \sum_{n=-N_U}^{n=N_U} V_n e^{in\alpha x}. \tag{3.7}$$

The lengths of these expansions can be calculated easily by noting that each modal shape function Φ_n is approximated by a polynomial of order K which leads to $N_U = K \cdot N_A + M$. In general, $N_U > M$ unless $K = 0$, which is clearly unacceptable.

The same velocity components can also be expressed using the discretized form of the solution, i.e.,

$$\begin{aligned} u_l(x) \equiv u(x,\ f(x)) &\cong u_0(f(x)) + \sum_{n=-M}^{n=M} D\Phi_n(f(x))e^{in\alpha x} \\ &= u_0(f(x)) + \sum_{n=-M}^{n=M}\sum_{j=0}^{j=K} G_j^n DT_j(f(x))e^{in\alpha x} \end{aligned} \tag{3.8a}$$

$$v_l(x) \equiv v(x,\ f(x)) \cong -i\alpha \sum_{n=-M}^{n=M} n\Phi_n(f(x))e^{in\alpha x} = -i\alpha \sum_{n=-M}^{n=M}\sum_{j=0}^{j=K} nG_j^n T_j(f(x))e^{in\alpha x}. \tag{3.8b}$$

Comparison of (3.7) and (3.8) permits specification of flow boundary conditions for each Fourier mode in terms of the unknown coefficients of the Chebyshev expansions.

Substitution of (3.6) into (3.8) shows a need for evaluation of $T_j(f(x))$ and $DT_j(f(x))$. Both these functions are periodic in x and can be expressed using the Fourier expansions

$$T_j(f(x)) = \sum_{k=-\infty}^{k=\infty} w_k^j e^{ik\alpha x}, \qquad DT_j(f(x)) = \sum_{k=-\infty}^{k=\infty} d_k^j e^{ik\alpha x}. \tag{3.9}$$

Use of the well-known recurrence relation for the Chebyshev polynomials

$$T_{j+1}(y) = 2yT_j(y) - T_{j-1}(y) \tag{3.10}$$

leads to the following expressions for the coefficients of $T_{j+1}(f(x))$:

$$w_k^{j+1} = 2\sum_{s=-\infty}^{s=\infty} A_k w_{k-s}^j - w_k^{j-1}. \tag{3.11}$$

The evaluations of these coefficients begins with

$$w_0^0 = 1, \quad w_k^0 = 0 \quad \text{for } k \geq 1; \qquad w_0^1 = A_0, \quad w_k^1 = A_k \quad \text{for } k \geq 1.$$

The differentiation of the general formula (3.10) yields

$$DT_{j+1}(y) = 2T_j(y) + 2yDT_j(y) - DT_{j-1}(y) \tag{3.12}$$

and leads to the following recurrence relation for the Fourier coefficients of $DT_{j+1}(f(x))$,

$$d_k^{j+1} = 2\sum_{s=-\infty}^{s=\infty} A_s d_{k+s}^j - d_k^{j-1} + 2w_k^j, \tag{3.13}$$

whose evaluation is initiated with

$$d_k^0 = 0 \quad \text{for } k \geq 0; \qquad d_0^1 = 1, \quad d_k^1 = 0 \quad \text{for } k \geq 1; \qquad d_0^2 = 4A_0, \quad d_k^2 = A_k \quad \text{for } k \geq 1.$$

Substitution of (3.9) into (3.2) leads to the Fourier expansions

$$\Phi_n(f(x)) = \sum_{k=-\infty}^{k=\infty}\sum_{j=0}^{j=K} G_j^n w_k^j e^{ik\alpha x}, \tag{3.14a}$$

$$D\Phi_n(f(x)) = \sum_{k=-\infty}^{k=\infty}\sum_{j=0}^{j=K} G_j^n d_k^j e^{ik\alpha x}, \tag{3.14b}$$

Insertion of (3.14) into (3.8) and separation of the Fourier modes result in the explicit expressions for coefficients of Fourier expansions (3.7), i.e.,

$$U_n = F_n + \sum_{m=-M}^{m=M}\sum_{j=0}^{j=K} d_{n-m}^j G_j^m, \tag{3.15a}$$

$$V_n = -i\alpha \sum_{m=-M}^{m=M}\sum_{j=0}^{j=K} m w_{n-m}^j G_j^m. \tag{3.15b}$$

The complex quantities F_n, $n = 0, 1, \ldots$, are the Fourier coefficients of the reference flow u_0 calculated along the line l, i.e.,

$$u_0(f(x)) = \sum_{n=-\infty}^{n=\infty} F_n e^{in\alpha x}. \tag{3.16}$$

In the case of the Poiseuille flow, the Fourier coefficients have the form

$$F_0 = 1 - \sum_{j=-N_A}^{j=N_A} |A_j|^2, \qquad F_n = -\sum_{j=-N_A}^{j=N_A} A_j A_{n-j}, \tag{3.17}$$

The actual range of the summation in (3.16) is $\pm 2 \cdot N_A$.

Let velocity field satisfy the following conditions imposed at the line l,

$$u_l(x) \equiv u(x, f(x)) = g_u(x), \qquad v_l(x) \equiv v(x, f(x)) = g_v(x), \tag{3.18}$$

where g_u and g_v are given, periodic functions with the period λ_x, which can be expressed, without loss of generality, as the Fourier expansions

$$g_u(x) = \sum_{n=-N_P}^{n=N_P} P_n e^{in\alpha x}, \qquad g_v(x) = \sum_{n=-N_P}^{n=N_P} R_n e^{in\alpha x}. \tag{3.19}$$

The number of terms in both of these expansions can be specified arbitrarily and has been assumed to be the same without loss of generality. In terms of the theory of square-integrable functions, conditions (3.18) are equivalent to the integral conditions

$$\int_x^{x+\lambda_x} [u_l(x) - g_u(x)] e^{-in\alpha x}\, dx = 0, \qquad \int_x^{x+\lambda_x} [v_l(x) - g_v(x)] e^{-in\alpha x}\, dx = 0, \quad |n| \geq 0$$

and can be expressed as

$$U_n = P_n, \qquad V_n = R_n, \quad n \geq 0. \tag{3.20}$$

Typically, one would select the first $M + 1$ conditions for U_n and V_n to close the system (3.5). We shall demonstrate that not all of conditions (3.20) are independent, however, and that specification of velocity components along the line l in (3.19) is not completely arbitrary, but has to satisfy a certain constraint.

Let ψ denote the stream function of the flow in the corrugated channel, i.e., $\psi = \Psi_0 + \Psi$, where Ψ_0 denotes the stream function of the reference flow. We can evaluate ψ along the line l, i.e., $\psi_l(x) = \psi(x, f(x))$. Clearly, ψ_l is a periodic function of x, i.e., $\psi_l(x) = \psi_l(x + \lambda_x)$. One can write the equality

$$\psi_l(x + \lambda_x) - \psi_l(x) = \int_x^{x+\lambda_x} \frac{d\psi_l(x)}{dx}\, dx = 0, \tag{3.21}$$

which, after differentiation of ψ_l as a composed function, yields

$$\int_x^{x+\lambda_x} \left\{ \frac{\partial \psi}{\partial x}(x,\, f(x)) + \frac{\partial \psi}{\partial y}(x,\, f(x)) \cdot f'(x) \right\} dx = 0. \tag{3.22}$$

The above formula can be rewritten in terms of velocity components specified at the line l as

$$\int_x^{x+\lambda_x} \{-g_v(x) + g_u(x) \cdot f'(x)\}\, dx = 0. \tag{3.23}$$

Substitution of (3.6) and (3.19) into (3.23) and integration of the resulting expression results in

$$R_0 = -i\alpha \sum_{n=-N_A}^{n=N_A} n P_n A_n^\star. \tag{3.24}$$

The above shows that the mean value of g_v, i.e., R_0, cannot be specified arbitrarily; this value results from specification of g_u as well as shape of the line $f(x)$, i.e., A_n. The summation in (3.24) extends between $n = \pm\min(N_P, N_A)$. Since N_P can be extended arbitrarily (i.e., the length of the Fourier expansions (3.19) can be arbitrarily increased by adding to them null terms), the limits of the summation are written as $\pm N_A$.

Similar arguments with g_u and g_v in (3.23) replaced by u_l and v_l, respectively, and with use of (3.7), lead to the conclusion that

$$V_0 = -i\alpha \sum_{n=-N_A}^{n=N_A} n U_n A_n^\star. \tag{3.25}$$

The above relation shows that V_0 is not an independent quantity but results from specification of U_n. The summation in (3.25) extends between $n = \pm\min(N_U, N_A)$. Since $N_U > N_A$, the limits of the summation are written as $\pm N_A$.

The flow boundary conditions can now be written as

$$U_n = F_n + \sum_{m=-M}^{m=M} \sum_{j=0}^{j=K} d_{n-m}^j G_j^m = P_n, \qquad M \geq n \geq 0, \tag{3.26a}$$

$$V_n = -i\alpha \sum_{m=-M}^{m=M} \sum_{j=0}^{j=K} m w_{n-m}^j G_j^m = R_n, \qquad M \geq n \geq 1. \tag{3.26b}$$

It can be shown that in the case of numerical implementation, when the calculations are carried out with the use of M Fourier modes for the stream function, the condition $V_0 = R_0$ is automatically satisfied when $M \geq N_P$. If $M < N_P$ but $N_A \leq M$, again this condition is automatically satisfied. Otherwise

$$R_0 = V_0 - \left(i\alpha \sum_{n=M+1}^{n=N_A} n P_n A_n^\star + \text{c.c.} \right), \tag{3.27}$$

which leads to a contradiction. Here, c.c. stands for the complex conjugate. The above discussion shows that, regardless of circumstances, no condition for V_0 can be imposed. One may note that in practical calculations an accurate solution can be obtained only when the length M of its Fourier representation (3.1) is larger than both N_A and N_P. In such cases the condition $V_0 = R_0$ is satisfied automatically.

Flow conditions (3.26) can be specified along any line periodic in x, and in particular, along the top and bottom walls of the channel, i.e., at $y_U(x)$ and $y_L(x)$. The problem to be solved numerically consists of $M+1$ fourth-order ordinary differential equations of type (2.7) supplemented by Eq. (3.26) applied at the top and bottom walls, which provides $4\cdot(M+1)-2$ out of the required $4\cdot(M+1)$ conditions necessary to close the system. The reader may note that these conditions are of internal type rather than boundary type and, indeed, no explicit relations between the values of the stream function and/or its derivatives are postulated at the boundaries of the computational domain (i.e., at $y=\pm 1$). Consequently, our system of ordinary differential equations is not supplemented explicitly by boundary conditions of any kind. The computed flow field extends over the whole computational domain, but only the part contained between the wall contours $y_U(x)$ and $y_L(x)$ has a physical meaning.

Equations (3.26) provide useful relations for evaluation of error in enforcement of flow conditions along the walls. Since both U_n and V_n are defined for $0 \le n \le N_U$ (see Eq. (3.7)) but flow conditions are imposed only for $0 \le n \le M$, the flow boundary conditions will not be satisfied exactly. Evaluation of (3.26) for $n > M$ gives information about the absolute value as well as spectral composition of the error. Since the method is spectrally accurate, this error should be decreasing exponentially with increasing M. The evaluation of the error is computationally very inexpensive because it involves only substitution of the already computed quantities. The simplicity in determination of the error permits a straightforward implementation of the algorithm in a self-adaptive mode, where the number of Fourier modes keeps increasing until the specified accuracy criteria are met.

To close the problem of flow through the channel, we need to specify two arbitrary conditions. This need arises due to the dependence of V_0 on other coefficients of Fourier expansions (3.7), as discussed above (see also discussion in Section 2). One of the required conditions is selected by specifying the average value of the stream function at the lower wall, i.e.,

$$\sum_{s=-M}^{s=M}\sum_{j=0}^{j=K} G_j^s \left(w_s^j\right)_L^\star = -(H_0)_L + T, \tag{3.28}$$

where T is the selected average value of the stream function, the subscript L denotes the values corresponding to the lower wall, and H_n stands for the coefficients of Fourier expansion of the stream function of the reference flow, i.e.,

$$\Psi_0(f(x)) \approx \sum_{n=-M}^{n=M} H_n e^{in\alpha x}. \tag{3.29}$$

The second condition is selected by specifying the average volume flux through the channel. The volume flux $Q(x)$ is a periodic function of x and can be represented as a Fourier

expansion in the form

$$Q(x) \approx \sum_{n=-M}^{n=M} Q_n e^{in\alpha x}. \tag{3.30}$$

The coefficients Q_n can be evaluated by integrating the x-velocity component $u(x, y) = u_0(y) + u_1(x, y)$ across the channel, i.e.,

$$Q(x) = \int_{y_L}^{y_U} (u_0 + u_1)\, dy = \Psi_0(y_U(x)) + \Psi(y_U(x)) - \Psi_0(y_L(x)) - \Psi(y_L(x)), \tag{3.31}$$

and substituting the relevant expressions for $\Psi_0(x)$ and $\Psi(x)$. The final form of the volume flux condition is

$$\sum_{s=-M}^{s=M} \sum_{j=0}^{j=K} G_j^s \left(w_s^j\right)_U^\star = Q_0 - (H_0)_U + T, \tag{3.32}$$

where Q_0 stands for the specified average volume flux (see Eq. (2.9)) and the subscript U denotes values evaluated at the upper wall.

Discussion of the treatment for the flow boundary conditions has been carried out so far in a rather general form that permits specification of both x and y (or tangential and normal to the wall) velocity components. In the case of a solid non-permeable wall considered in Section 2, these conditions can be written in a simpler form, i.e.,

$$F_n + \sum_{m=-M}^{m=M} \sum_{j=0}^{j=K} d_{n-m}^j G_j^m = 0, \qquad M \geq n \geq 0, \tag{3.33a}$$

$$\sum_{m=-M}^{m=M} \sum_{j=0}^{j=K} m w_{n-m}^j G_j^m = 0, \qquad M \geq n \geq 1, \tag{3.33b}$$

with (3.28) and (3.32) unchanged. In this case, the stream function is constant and equal to T along the lower wall (see Eq. (2.9)).

Equations (3.5), (3.28), (3.22), and (3.33) form a complete nonlinear algebraic system for the unknown coefficients G_j^n, $j = 0, \ldots, K$, $n = 0, \ldots, M$. This system was solved iteratively by taking advantage of the structure of the original differential system. The reader may note that the coupling between the differential equations (2.7) is only due to nonlinear terms and that Φ_0 appears in these equations in a very special way. To illustrate this point, we write Eqs. (2.7) in the form

$$\begin{aligned} &\left\{D_n^2 - in\alpha \operatorname{Re}\left\lfloor (u_0 + D\Phi_0) D_n - D^2(u_0 + D\Phi_0)\right\rfloor\right\} \Phi_n \\ &\quad = \Theta_n(\Phi_1, \Phi_1^\star, \Phi_2, \Phi_2^\star, \ldots), \qquad n \geq 1, \end{aligned} \tag{3.34}$$

$$D^4 \Phi_0 = -2\alpha \operatorname{Re} \operatorname{Im} \left\{ \sum_{n=1}^{\infty} n \left(D\Phi_n^\star D^2 \Phi_n + \Phi_n^\star D^3 \Phi_n \right) \right\}. \tag{3.35}$$

The right-hand side of (3.34) contains the nonlinear terms but does not contain Φ_0 and Φ_n.

In the above, the modal functions with negative indices have been replaced by their complex conjugates. The discrete system (3.5) supplemented by (3.28.), (3.32), and (3.33) can be written in analogous form as

$$\mathbf{L}_n\mathbf{G}^n = \mathbf{R}_n\big(G_0^1, G_1^1, \ldots, G_K^1; \ldots; G_0^{n-1}, G_1^{n-1}, \ldots, G_K^{n-1}; G_0^{n+1}, G_1^{n+1}, \ldots, G_K^{n+1}; \ldots; G_0^M, G_1^M, \ldots, G_K^M\big), \qquad n = 0, \ldots, M. \quad (3.36)$$

In the above, $\mathbf{L}_n$ denotes the discretization matrix of the linear differential operators from the left-hand side of (3.34) (for $n \geq 1$) and (3.35) (for $n = 0$). This matrix also includes four rows containing coefficients corresponding to $G_0^n, \ldots, G_K^n$ in (3.28), (3,32), and (3.33). $\mathbf{G}^n$ stands for the vector of the unknown Chebyshev coefficients $G_0^n, \ldots, G_k^n$. $\mathbf{R}_n$ stands for the vector corresponding to discretization of the nonlinear operator Θ_n. This vector includes four entries corresponding to the parts of (3.28), (3,32), and (3.33) that are not included in $\mathbf{L}_n$. The above form of the discretized system demonstrates that the linear part of (3.5), (3.28), (3.32), and (3.33) can be split into $M + 1$ separate linear subsystems, assuming that the couplings due to nonlinearity and due to boundary conditions (which are placed in the right-hand side vectors) are known. In this study, the right-hand sides were calculated using information from the previous iteration and the subsystems were solved in descending order starting with the subsystem corresponding to $n = M$. The iterations were continued until the change in the magnitude of the modal functions was less than the prescribed convergence criterion ε. Most of the results presented in this paper were obtained with the machine accuracy level and thus the convergence criterion was set to be $\varepsilon = 10^{-14}$. The number of the required iterations in most cases would be less than 50. The Chebyshev representations of the nonlinear terms were calculated directly using exact formulas for manipulation of Chebyshev polynomials. In general, the number of Fourier modes required to produce a solution with the desired accuracy (machine accuracy in this case) is not known in advance. The computations were thus carried out in a self-adaptive mode, where the solution would be recomputed with the increasing number of modes M until the norm of the highest modal function reached a magnitude smaller than the desired accuracy (machine accuracy in the present case). This "continuation strategy" usually reduces efficiency of the calculations but improves convergence properties of the iterative scheme.

The implementation of the algorithm described in this paper involves subtraction of the reference flow, e.g., Eq. (2.3). This step is not required in general and a version of the algorithm that solves for the complete flow can be easily worked out.

4. TESTING OF THE ALGORITHM

In this section, we shall discuss the results of numerical testing of the algorithm. We shall demonstrate the spectral accuracy of the flow field approximation and discuss how changes of different available parameters affects this accuracy. All tests discussed have been carried out for the Reynolds number $\mathrm{Re} = 100$ unless otherwise noted. For simplicity, the upper wall of the channel has been assumed to be flat, i.e., $y_U = 1$, while the shape of the bottom wall has been taken as

$$y_L(x) = -1 + H_L + H_L \cdot \cos(\alpha x), \quad (4.1)$$

i.e., it contains only one Fourier mode. The reader may note that the shape of the bottom wall is completely described by two parameters, i.e., the wavenumber α and the amplitude H_L. It is of interest to know how the variations of H_L and α can affect the absolute accuracy of the calculations.

In order to demonstrate the spectral accuracy of the algorithm, two aspects of the approximation should be considered. For the y-direction, the Chebyshev expansions (3.2) with coefficients calculated from the Galerkin conditions (3.5) are guaranteed to be spectrally accurate with the increasing number of terms K. We have found that in most cases sixty Chebyshev polynomials provided machine accuracy. This number needs to be increased for $\alpha \to \infty$ (shorter waves), especially when higher Fourier modes begin to play a significant role in the solution. This need for an increased number of Chebyshev polynomials under such conditions can be explained by noting that each amplitude function Φ_n develops a boundary layer near $y = -1$ as $\alpha \to \infty$. These layers are extremely thin for larger values of α and for higher Fourier modes (see Fig. 2). Inside the layers the functions Φ_n and their derivatives change rapidly, while in the rest of the domain they assume values very close to zero. In order to obtain the required resolution near $y = -1$, and in order to avoid the (numerical) oscillations in the distributions of Φ_n outside the boundary layers, the truncated Chebyshev expansions (3.2) must contain a larger number of terms. Typically, $K \approx 80$ for $\alpha = 20$, and $K \approx 160$ for $\alpha = 50$.

The second aspect of the spectral accuracy involves the convergence of the truncated Fourier series describing x-variations of the flow field. In all tests dealing with this issue, the number of Chebyshev polynomials K was kept sufficiently large so that the associated discretization error was reduced to machine accuracy level. The errors to be discussed below

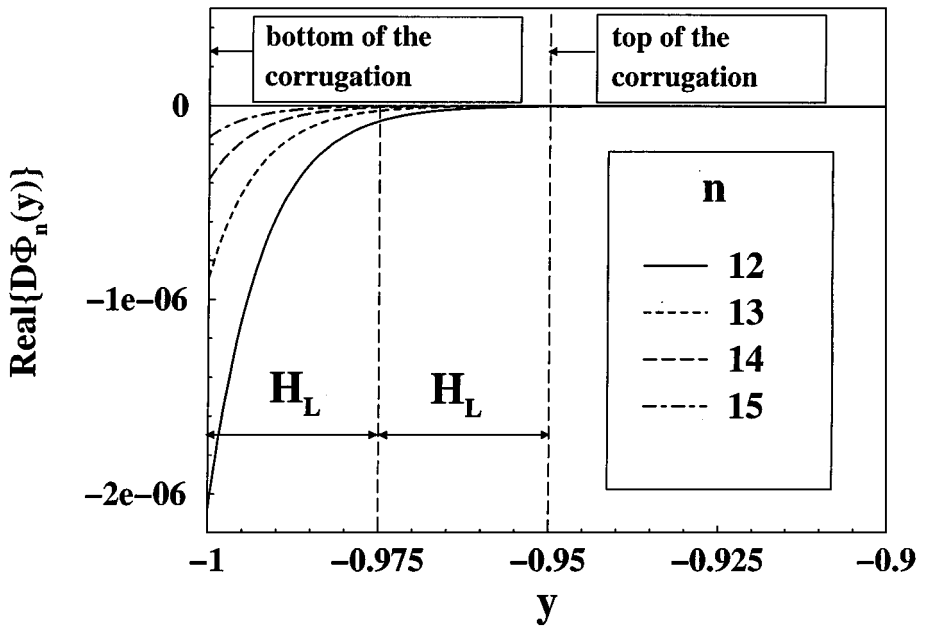

FIG. 2. Distribution of the real part of the derivative of the amplitude function $D\Phi_n$ as a function of y for higher modes ($n > 11$) in the area close to the lower wall for $\alpha = 10$ and $H_L = 0.025$. Formation of boundary layers, which are completely contained within a strip of thickness equal to the maximum height of the corrugation (i.e., $2H_L$), is clearly visible for each amplitude function.

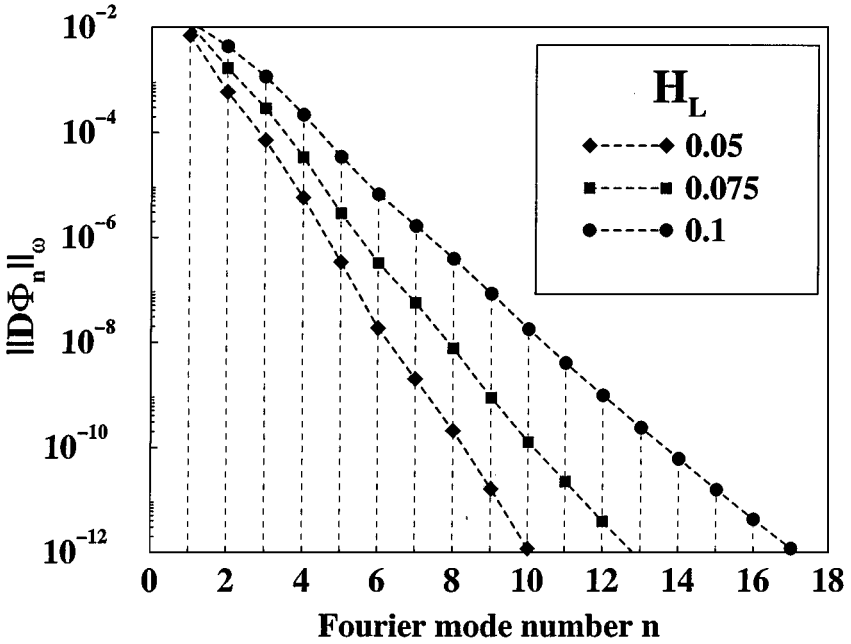

FIG. 3. Variations of the Chebyshev norm (4.2) of the derivative $D\Phi_n$ as a function of the mode number n for $\alpha = 1$. Calculations have been carried out with $M = 20$ Fourier modes.

occur solely due to truncation of the Fourier series.

Figure 3 displays variations of the Chebyshev norm of the first derivative of the amplitude function $D\Phi_n$ as a function of the Fourier mode number n. The norm decreases as a function of n with the rate of the decrease very rapidly reaching (asymptotically) exponential form. The Chebyshev norm used in the testing is defined as

$$\|D\Phi_n\|_\omega = \left\{ \int_{-1}^{1} D\Phi_n(y) \cdot D\Phi_n^\star(y)\omega(y)\, dy \right\}^{1/2}, \tag{4.2}$$

where ω denotes the Chebyshev weight function $\omega(x) = (1 - x^2)^{1/2}$. The derivatives $D\Phi_n$ rather then the functions Φ_n have been selected as the test quantities because they directly correspond to the Fourier representation of the x-component of velocity vector.

The accuracy of enforcement of flow boundary conditions (2.8) is crucial for the proposed algorithm. Components of velocity vector evaluated at the lower wall $u_L(x) \equiv u(x, y_L(x))$ and $v_L(x) \equiv v(x, y_L(x))$ should satisfy conditions (2.8). However, in numerical implementation only the first M Fourier modes are set to zero, as discussed in Section 3 (see Eq. (3.33)). The rest of the available Fourier modes (for $M + 1 \le n \le N_U$) evaluated at the lower wall provide a convenient measure of the magnitude and spectral composition of the error. This error can be evaluated easily from Eq. (3.15) through a simple substitution of the already computed quantities. In the tests discussed below, u_L and v_L were computed using 50 modes ($M < 50 < N_U$), which was sufficient to provide machine accuracy.

The error in enforcement of flow boundary conditions can be measured by introducing two norms, i.e., the L_∞-norm and the L_2-norm, and applying them to both velocity components

evaluated at the lower wall. These norms are defined as

$$\|u_L(x)\|_\infty := \sup_{0\le x\le 2\pi/\alpha} |u(x, y_L(x))|, \qquad \|v_L(x)\|_\infty := \sup_{0\le x\le 2\pi/\alpha} |v(x, y_L(x))|, \quad (4.3a)$$

$$\|u_L(x)\|_2 := \left(\int_x^{x+\lambda_x} |u(x, y_L(x))|^2 \, dx \right)^{1/2}, \qquad \|v_L(x)\|_2 := \left(\int_x^{x+\lambda_x} |v(x, y_L(x))|^2 \, dx \right)^{1/2}. \quad (4.3b)$$

The first norm is of greater interest in assessing the error of the method and thus is used in the discussion that follows. The second norm gives qualitatively similar results with the numerical values being approximately 10 times smaller than the corresponding values of the first norm.

Figure 4 displays variations of $\|u_L\|_\infty$ and $\|v_L\|_\infty$ as a function of the total number of Fourier modes M used for the stream function approximation. The reader may note that the magnitude of contributions of the higher modes decreases exponentially. The distributions of $u_L(x)$ and $v_L(x)$ over a single period are shown in Fig. 5. Both functions are oscillatory in x with maxima located close to $x = \pi$, i.e., around the bottom of the corrugation. The fact that the maximum error in enforcement of flow boundary conditions occurs at the bottom can be explained by noting that all amplitude functions Φ_n, $n \ge 1$ attain their maxima (in both real and imaginary parts) at or very near to $y = -1$. One can expect therefore that contributions of higher Fourier modes are relatively more important at these particular locations, and thus the rate of error reduction as a function of the total number of Fourier

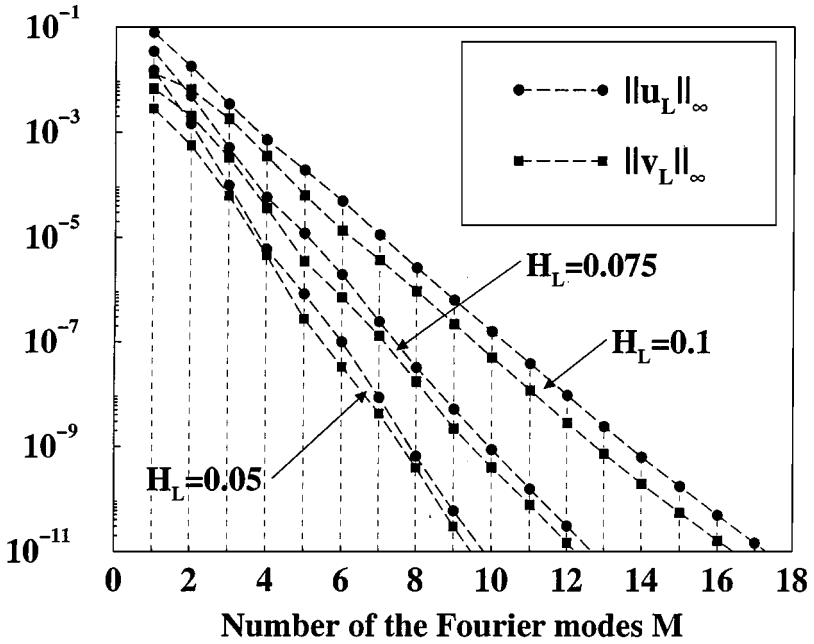

FIG. 4. Variations of the L_∞-norm (4.3a) of the (x, y) components of velocity vector evaluated at the lower wall $u_L = u(x, y_L(x))$, $v_L = v(x, y_L(x))$ as a function of the total number of Fourier modes M used in the calculations for $\alpha = 1$.

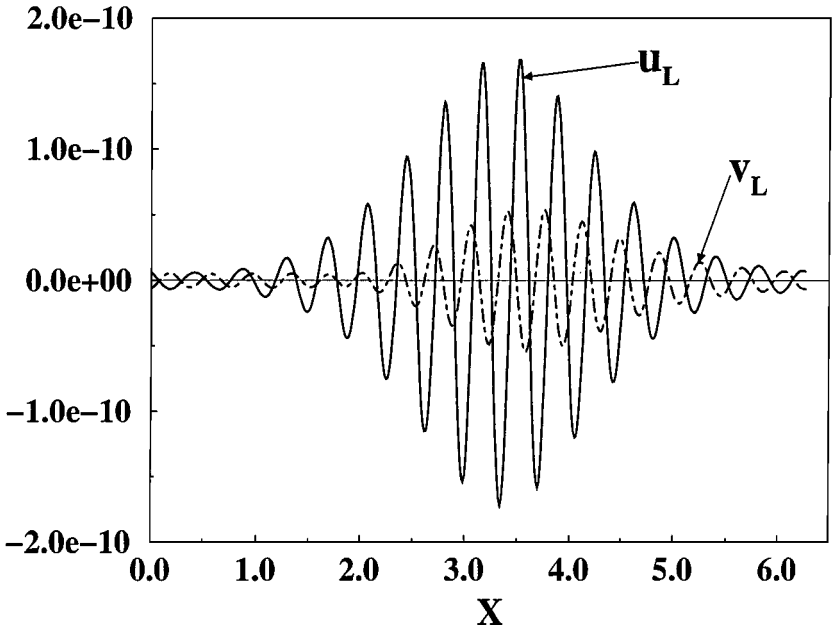

FIG. 5. The (x, y)-components of velocity vector evaluated at the lower wall $u_L = u(x, y_L(x))$, $v_L = v(x, y_L(x))$ for $\alpha = 1.0$, $H_L = 0.05$ with $M = 15$ Fourier modes used in the calculations.

modes M would be smaller in the vicinity of the bottom of the corrugation as compared to its top. This effect is more pronounced for large wavenumbers α due to the fact that boundary layers appearing in the distributions of Φ_n's with a sufficiently large index n are thinner then the total depth of the wall corrugation $2H_L$ (see Fig. 2).

According to the implementation of boundary conditions (2.8), the Fourier spectrum of both components of velocity vector evaluated at the wall (see Fig. 5) should not contain any harmonics of order lower then the number of Fourier modes used in the calculations ($M = 15$ in this case). This property of the solution provides a useful test for accuracy and consistency of the algorithm. Results shown in Fig. 6 confirm that indeed the first 15 Fourier modes have been eliminated. These can be estimated on the basis of these results that, for the conditions used in this particular example, calculation with $M \geq 25$ modes should provide results with accuracy of machine arithmetic.

A series of calculations have been carried out in order to demonstrate that the assumed form of solution (2.6) is sufficiently general, at least for the range of parameters considered in this work. In principle, the stream function can either contain subharmonics or be quasiperiodic with respect to the x-variable. Although it is possible that such solutions may exist in our model problem for certain parameter settings, they have not been found in any of the test calculations. As an illustration, we shall consider three cases of the same flow with corrugation amplitude $H_L = 0.05$ and corrugation wavelength $\lambda_x = 2\pi/3$. In case A, the bottom wall was assumed to have the shape of the principal Fourier mode with the wavenumber $\alpha = 3$ and the relevant calculations were carried out using $M = 10$ Fourier modes. In case B, the same shape was assumed to be represented by the second Fourier mode (the principal mode has the wavenumber $\alpha = 1.5$), while in case C it was represented by the third Fourier mode (the principal mode has the wavenumber $\alpha = 1$). In order to have fully equivalent representations, the number of Fourier modes used in cases B and C was $M = 20$ and $M = 30$, respectively. The selected representations admitted subharmonics of

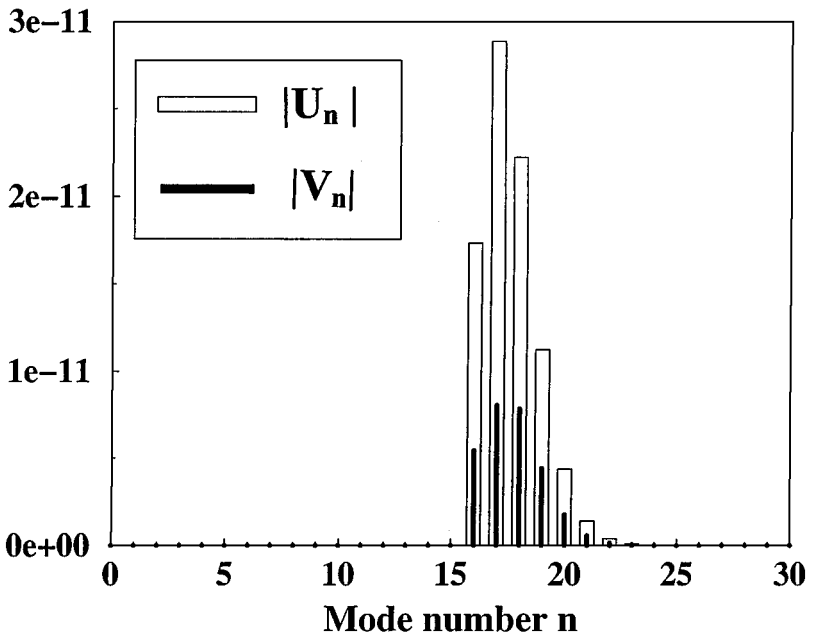

FIG. 6. Fourier spectra of distributions of u_L and v_L shown in Fig. 5. The reader may note the absence of the first 15 modes.

$\frac{1}{2}$ type in case B and subharmonics of $\frac{1}{3}$ type in case C. In all three cases calculations were initiated with three different initial approximations containing all Fourier modes and in all cases the solution process resulted in equivalent solutions. In cases B and C all subharmonics vanished during the iteration process. Figure 7, which displays the Fourier spectra of the x-component of velocity vector evaluated at the lower wall $u_L(x)$, demonstrates that solutions obtained in all three cases are identical.

The dependence of the boundary error on the shape parameters α and H_L, for a fixed number M of Fourier modes, has been also investigated. The norm $\|u_L\|_\infty$ was used as a measure of the error. Figure 8 illustrates variations of this norm as a function of the amplitude H_L while Fig. 9 shows variations of this norm as a function of the wavenumber α. The available results suggest that the error is at the machine accuracy level for H_L and α smaller then certain critical values. Once these values are reached, the error begins to increase rapidly in a somewhat universal manner. The universal (asymptotic) error behavior for increasing H_L can be approximated by a simple power law formula $\|u_L\|_\infty \approx H_L^{\beta_H}$, where the exponent β_H depends on the wavenumber α and the number of Fourier modes M used. The universal (asymptotic) error growth as a function of increasing α can be expressed by a similar power law, i.e., $\|u_L\|_\infty \approx \alpha^{\beta_\alpha}$, where the exponent β_α depends on the amplitude H_L and the number of Fourier modes M used. The available numerical results suggest that $\beta_H \approx M+2$ and $\beta_\alpha \approx M+1$. Careful analysis of Figs. 8 and 9 shows that increasing the number of Fourier modes M delays the onset of the asymptotic error growth (as H_L and α increase), but once the critical values of H_L and α are reached, the error growth is more rapid. This error behavior suggests a very rapid increase in the strength of nonlinear effects once a certain threshold in α and H_L is reached.

One additional issue might be important from a practical point of view; i.e., how many modes M should be used in order to capture, say, 99% of the "total information" regarding the flow field. Before an answer can be given, the concept of "information content" needs to

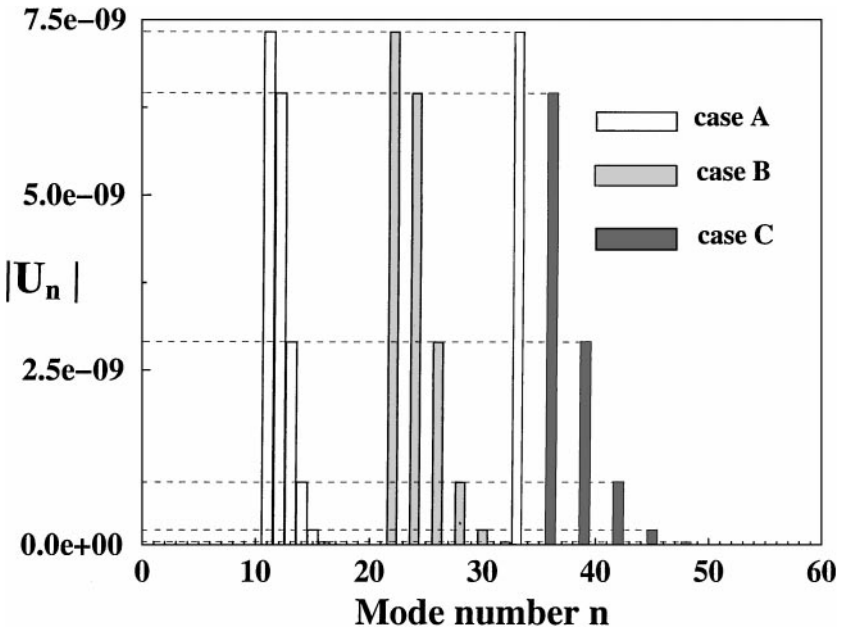

FIG. 7. Fourier spectra of the x-component of velocity vector evaluated at the lower wall, $u_L = u(x, y_L(x))$, calculated for the amplitude $H_L = 0.05$ and the wavelength $\lambda_x = 2\pi/3$, using three different forms of Fourier expansion. Case A: only basic harmonics are included ($\alpha = 3.0$, $M = 10$). Case B: 1/2-subharmonics are admissible ($\alpha = 1.5$, $M = 20$). Case C: 1/3 subharmonics are admissible ($\alpha = 1.0$, $M = 30$). The reader may note the absence of any subharmonics in the solution.

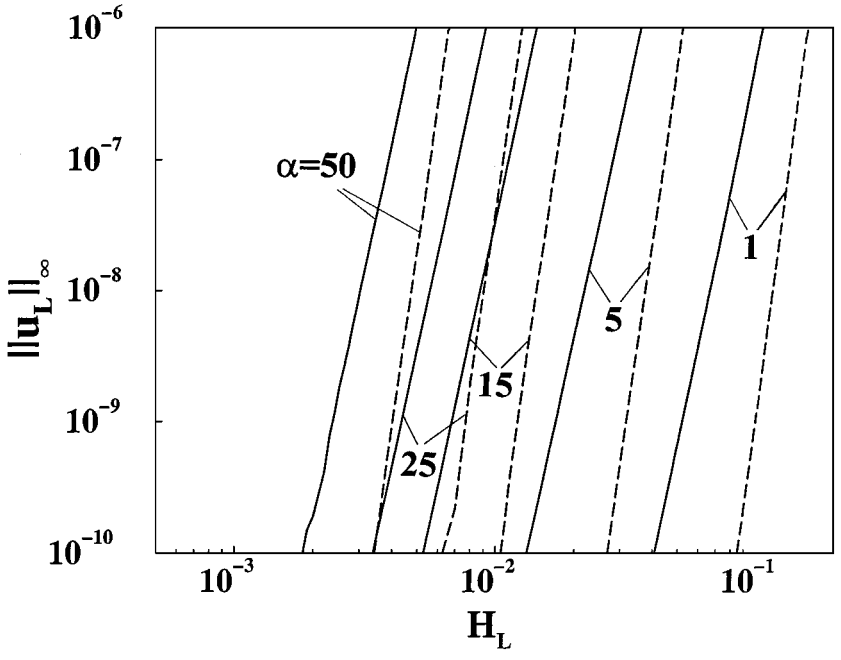

FIG. 8. The L_∞-norm (Eq. 4.3a) of the x-component of velocity vector evaluated at the lower wall, $u_L = (x, y_L(x))$, as a function of the amplitude H_L of the wall corrugation, plotted for different values of the wavenumber α and evaluated using either $M = 8$ (solid lines) or $M = 12$ (dashed lines) Fourier modes. Since the expected value is zero, the magnitude of this norm provides a measure of error in enforcement of flow boundary conditions.

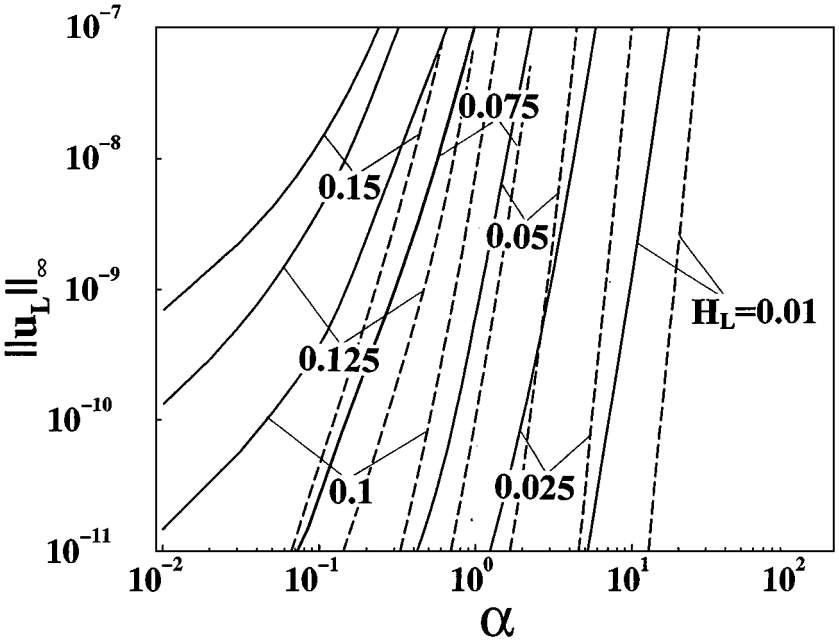

FIG. 9. The L_∞-norm (Eq. 4.3a) of the x-component of velocity vector evaluated at the lower wall, $u_L = (x, y_L(x))$, as a function of the wavenumber α, plotted for different values of the amplitude H_L evaluated using either $M = 8$ (solid lines) or $M = 12$ (dashed lines) Fourier modes. Since the expected value is zero, the magnitude of this norm provides a measure of error in enforcement of flow boundary conditions.

be precisely defined. For example, one may consider the kinetic energy $E_K(M)$ contained in the first M Fourier modes as an appropriate measure, and then the information content can be defined as $I(M) := E_K(M)/E_K(\infty)$. The symbol $E_K(\infty)$ denotes the kinetic energy of the actual solution, which, in general, may not be known. However, one can expect that the calculated value of $E_K(M)$ converges to a certain limit with $M \to \infty$; this limit can be approximately determined by carrying out calculations for increasing M, until the difference $|E_K M) - E_K(M-1)| < \varepsilon$, where ε is a small, positive number.

Kinetic energy represents only one of many possible measures. A reasonable alternative is offered, for example, by the mean pressure drop along the corrugated wall. Various other quantities have also been investigated, leading to the conclusion that the best measure is offered by quotients based on velocity components. The measures of information content adopted in this analysis are thus defined as

$$I_U(M) = \frac{\|u\|_H(M)}{\|u\|_H(\infty)}, \qquad I_V(M) = \frac{\|v\|_H(M)}{\|v\|_H(\infty)}, \tag{4.4}$$

where each component of the velocity field is considered separately, and the norm $\|\cdot\|_H$ is defined as

$$\|D\|_H = \left\{ \int_0^{2\pi/\alpha} \left[\int_{-1}^{1} |D(x,y)|^2 \omega(y)\, dy \right] dx \right\}^{1/2}. \tag{4.5}$$

The norm (4.5) arises naturally from the mathematical context of the proposed method,

which involves construction of the solution in the Hilbert space spanned by the set of functions

$$B_F = \{b_{j,n}(x, y) = T_j(y) \exp(in\alpha x),\ j \geq 0,\ |n| \geq 0\},$$

which are orthogonal in the following sense:

$$\langle b_{j,k}, b_{m,n} \rangle_H \equiv \int_0^{2\pi/\alpha} \left[\int_{-1}^{1} b_{j,k}(x, y) b^{\star}_{m,n}(x, y) \omega(y)\, dy \right] dx = 0, \qquad \text{for } j \neq m \quad \text{or} \quad k \neq n.$$

The numerical tests have shown that the "information measures" (4.4) provide more restrictive criterion of convergence than those based on either the kinetic energy or pressure gradient. In other words, high information content in the sense of (4.4) guarantees that physically relevant characteristics of the flow field are calculated with high accuracy. In should be noticed that none of the possible definitions of the quotients $I(M)$ may guarantee that $I(M)$ is monotonically increasing and upper bounded by unity, which means that $I_U(M)$ and $I_V(M)$ are not, in a literal sense, information content measures. We have found, however, that such exceptional cases occur very seldom. Most common behavior is illustrated in Fig. 10, which displays the quotients $I_U(M)$ and $I_V(M)$ calculated for the amplitude $H_L = 0.02$ and for several values of the wavenumber α. Similarly, Fig. 11 shows the quotients $I_U(M)$ and $I_V(M)$ calculated for the wavenumber $\alpha = 10$ and different values of the amplitude H_L. In both cases the same tendency is observed; i.e., an increase of either α or H_L increases the strength of nonlinear effects and necessitates use of a larger number of Fourier modes. The reader may use these graphs to estimate the number of Fourier modes M required to guarantee that the solution captures at least, say, 95% of the total information content.

All tests discussed so far have been carried out for the lower wall represented by a single Fourier mode (see Eq. (4.1)). The formulation of the algorithm is, however, general and it can deal with shapes of both walls represented in terms of an arbitrary number of Fourier modes. Figure 12 displays streamline pattern associated with the flow in a channel whose walls have the shape given by

$$y_L(x) = -0.85 + [(0.04 \cdot e^{i\alpha x} + 0.01 \cdot e^{i2\alpha x} + 0.025 \cdot e^{i3\alpha x}) + \text{c.c.}],$$
$$y_U(x) = -0.85 + [(0.0125 \cdot e^{i\alpha x} + 0.0375 \cdot e^{i2\alpha x} + 0.025 \cdot e^{i3\alpha x}) \cdot e^{i2\pi/3} + \text{c.c.}],$$

with the wavenumber $\alpha = 1.0$ and calculated using $M = 24$ Fourier modes.

5. LIMITATIONS OF THE ALGORITHM

The flow problem is well posed in the flow domain, but its nature in the extended computational domain is not known. The proposed algorithm relies on the assumption that the solution to the flow problem can be extended to a larger computational domain and that this extension is sufficiently smooth. If this extension contains singularities, the proposed method will fail to deliver the expected accuracy and, in fact, it may fail to converge at all.

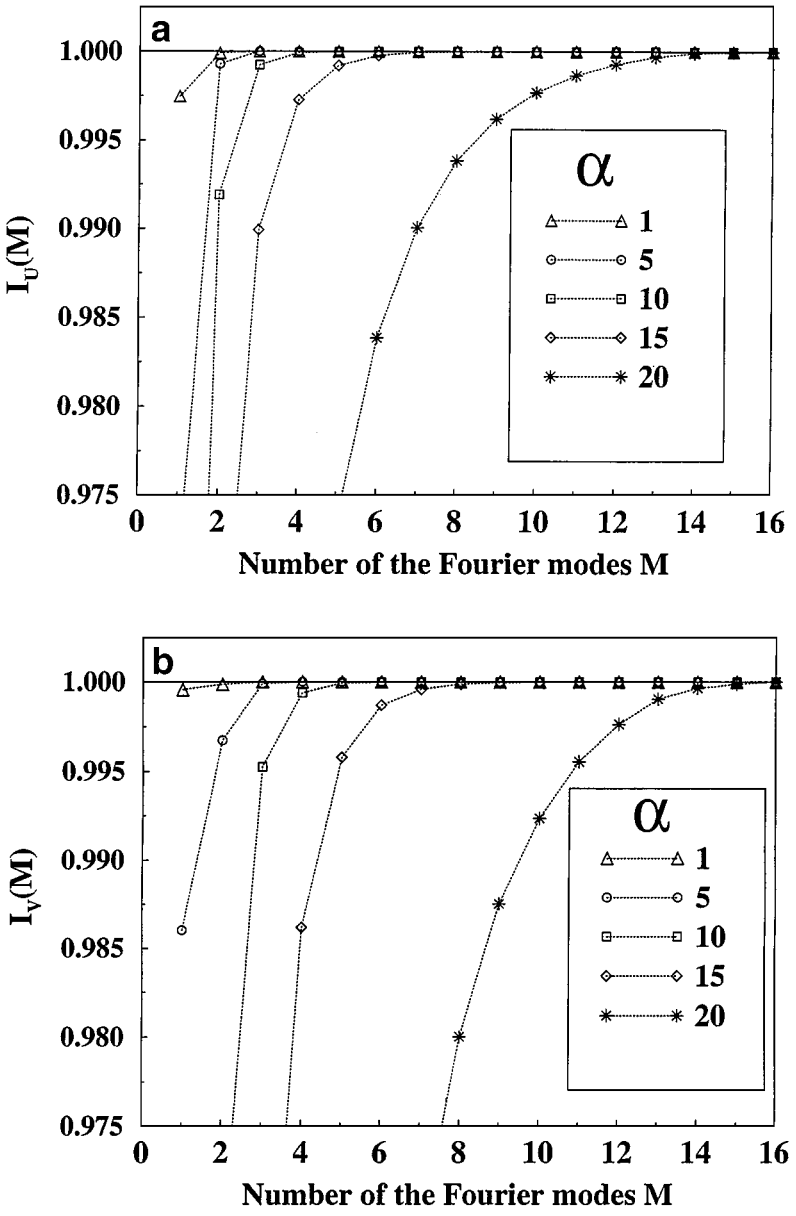

FIG. 10. The information content quotients I_U (a) and I_V (b) defined by Eq. (4.4) as a function of α for $H_L = 0.02$.

The potential difficulties can be illustrated using two simple examples. We shall begin with a one-dimensional boundary value problem

$$x^2F''(x) + xF'(x) - F(x) = 0, \qquad F(0.1) = A, \quad F(1) = B, \tag{5.1}$$

whose solution in the form

$$F(x) = \frac{10}{99}(10B - A)x + \frac{1}{99}(10A - B)\frac{1}{x} \tag{5.2}$$

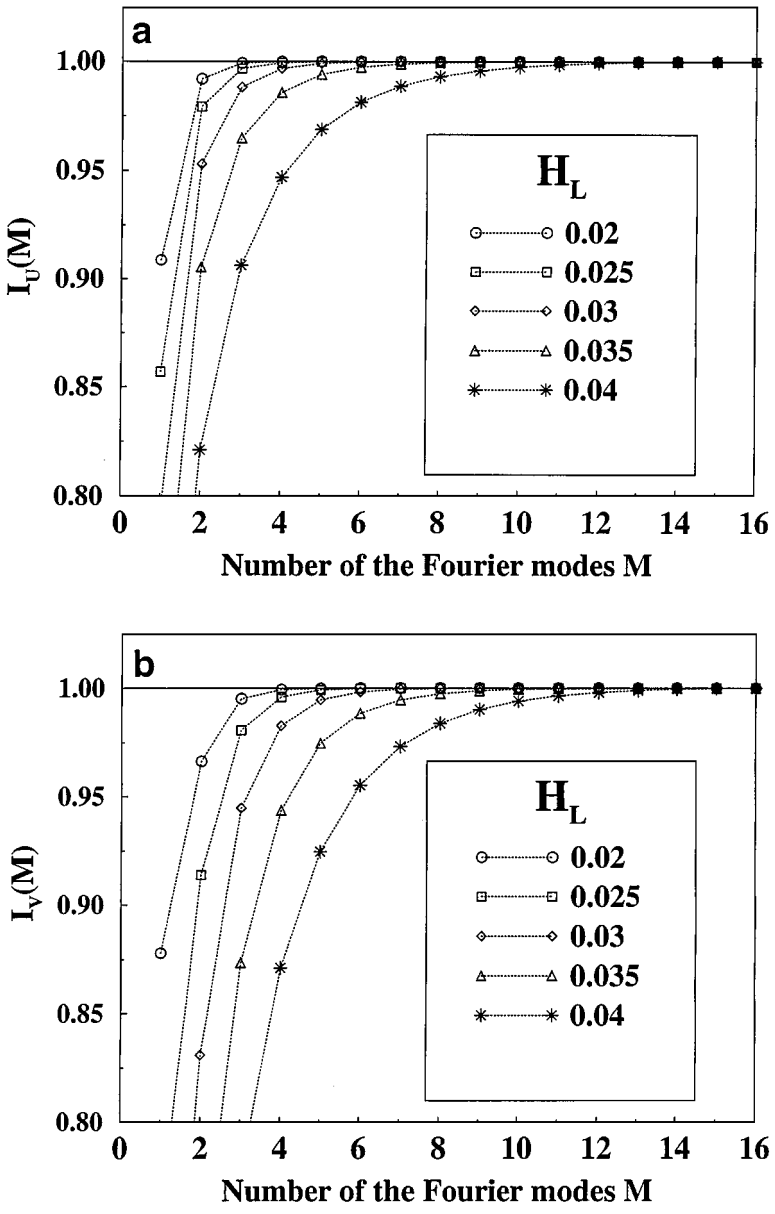

FIG. 11. The information content quotients I_U (a) and I_V (b) defined by Eq. (4.4) as a function of H_L for $\alpha = 10.0$.

is infinitely smooth in [0.1, 1]. We wish to solve this problem by approximating the solution in the extended domain [0, 1] and imposing condition at $x = 0.1$ as an internal condition rather then as a boundary condition. Obviously the solution cannot be smoothly extended to [0, 1] because of singularity at $x = 0$. The smooth extension is only possible for the very special case of $B = 10A$, but even then an arbitrary small change of the boundary data would create a singularity in the extended solution at $x = 0$. This means that a method based on spectral discretization in the extended domain should fail to converge.

The second example is more closely connected to the flow problem discussed in this study and involves the Dirichlet problem for the Laplace equation formulated for the

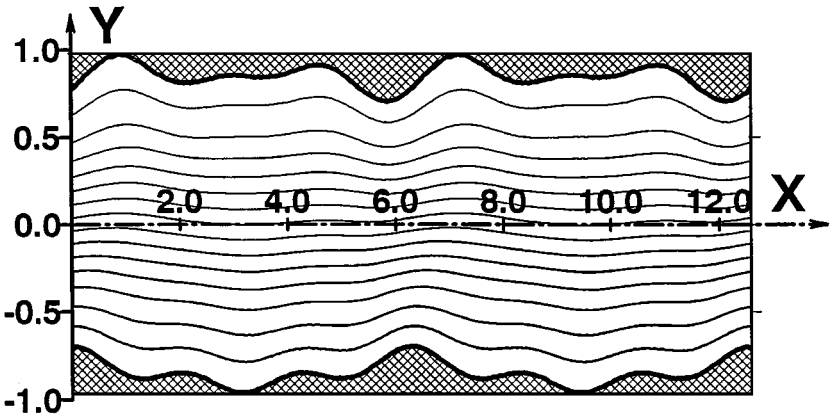

FIG. 12. Flow pattern in the channel with the lower wall located at $y_L = -0.85 + [(0.04e^{i\alpha x} + 0.01e^{i2\alpha x} + 0.025e^{i3\alpha x}) + \text{c.c.}]$ and the upper wall located at $y_U = 0.85 + [(0.0125e^{i\alpha x} + 0.0375e^{i2\alpha x} + 0.025e^{i3\alpha x})e^{i2\pi/3} + \text{c.c.}]$ for $\text{Re} = 20$.

x-periodic domain shown in Fig. 1b. The boundary conditions are assumed to be periodic and the problem can be stated as

$$\begin{gathered}\Delta F = 0 \quad \text{in } D, \quad F(x,-1) = g_L(x), \quad F(x, y_U(x)) = g_U(x), \\ F(0,y) = F(2\pi, y) \quad \text{for } y \in [-1,1],\end{gathered} \tag{5.3}$$

where, for simplicity, the lower wall is assumed to be flat. In the above, D denotes flow domain. We shall consider extended, regular computational domain $[0, 2\pi] \times [-1, 1]$ and seek the approximate solution F_e in the form of Fourier–Chebyshev series, i.e.,

$$F_e(x,y) = \sum_n \sum_k (c_{n,k}\cos(nx) + s_{n,k}\sin(nx))T_k(y). \tag{5.4}$$

We shall denote the difference between the extended and original domains as $D^\star$. Restriction of F_e (defined in $D + D^\star$) to D represents a solution F of the original problem. We shall demonstrate that the above representation of the solution is, in general, not acceptable.

Consider a function F that is harmonic everywhere in D, but the extension of which is singular at an arbitrarily selected point in $D^\star$. Because of the presence of singularity, this function cannot be represented by the Fourier expansion (5.4). The reader may note that Eq. (5.4) (with properly selected coefficients) represents nevertheless a certain harmonic function in $D + D^\star$. It can be shown that function of this form can approximate F in D with a prescribed accuracy (in the sense of sup-norm). This approximation may not be very accurate in $D^\star$ but this is irrelevant. To see that, map conformally the extended domain in such a way that D maps onto an annular region. The function F, expressed in new variables, can be expanded in a Laurent series whose upper radius of convergence is determined by the distance between the mapped singularity and the origin. Appropriate truncation of these series from above produces approximation of F with the desired accuracy in the image of D in the transformed domain. The resulting harmonic function F' can be extended arbitrarily far from the origin. The inverse mapping sends F' back to $D + D^\star$ where it approximates function F in D (but not in $D^\star$) with the same accuracy. Since F'

is harmonic in the entire extended domain, its representation in the form (5.4) exists and is spectrally convergent. Since F' approximates F in the whole extended domain, it must grow very rapidly in $D^\star$; this growth is more rapid when the error of the approximation is reduced. This means that the rate of convergence of the Fourier–Chebyshev series, despite the fact that it is spectral, is very slow, particularly in those parts of $D^\star$ which are located in the vicinity of the singularity. Increased accuracy requirements imply slower rate of convergence and necessitate use of an extremely large number of terms. This may make the method impractical in applications.

The above examples illustrate situations when the proposed algorithm fails. General conditions that guarantee the required smoothness of the extended solution of the Navier–Stokes equations, and thus guarantee appropriate performance of the proposed algorithm, are not known. In all cases considered in the present study, no failure has been encountered. Since the failure of the algorithm manifests itself either by the loss of convergence or by a very slow convergence, the reliability of the results can be tested a posteriori using convergence studies. If the algorithm is diagnosed as unreliable for a particular flow problem, one has no choice but to limit calculations to the physical domain and to rely on either a numerical coordinate generation or an analytical mapping that transforms the corrugated physical domain into a regular computational domain. Such tests have been done in the present study and the results obtained agreed with those produced using the direct approach.

6. CONCLUSIONS

An algorithm for a direct, spectrally accurate solution of the Navier–Stokes equations in domains with corrugated boundaries has been proposed. The algorithm eliminates the need for the coordinate generation and/or premapping required for regularization of the computational domain in standard implementation of spectral discretizations. The flow problem is posed for computational purposes as an internal problem rather than a boundary value problem, with the flow boundary conditions specified along a line that weaves through the interior of the computational domain. The discretization is based the Chebyshev expansions in the normal-to-the-wall direction and the Fourier expansions in the direction along the wall. Flow boundary conditions for each Fourier mode are expressed directly in terms of coefficients of Chebyshev expansions by using composite function formulation. The explicit expressions provided for evaluation of error in enforcement of flow boundary conditions permit implementation of the algorithm in a self-adaptive mode based on prescribed error bounds.

Various tests confirm that the algorithm delivers spectral accuracy. The absolute magnitude of the error (when the number of Fourier modes is kept constant) increases with increase of both the wavenumber α and the amplitude H of the wall corrugation. This growth becomes proportional to a certain power of α and H for a large enough α and H. Variations of the error suggest a rapidly increasing strength of nonlinear effects and the need to use a large number of Fourier modes when α and H reach a certain threshold.

The algorithm relies of the existence of a sufficiently smooth extension of the flow solution to the complete computational domain. Conditions that guarantee existence of such an extension are presently not known and caution is advised when applying the algorithm to new classes of problems.

ACKNOWLEDGMENTS

This work has been carried out with support of the NSERC of Canada, Canadair, and de Havilland.

REFERENCES

1. R. Balasubramian and S. A. Orszag, Numerical simulation of flow over wavy walls (AIAA Paper 80-1350), in *13th Fluid and Plasma Dynamics Conference, 1980*.
2. B. Benjamin, Shearing flow over a wavy boundary, *J. Fluid Mech.* **6**, 161 (1959).
3. C. Canuto, M. Y. Hussaini, A. Qurteroni, and T. A. Zang, *Spectral Methods in Fluid Dynamics* (Springer–Verlag, Berlin/New York, 1988).
4. E. A. Caponi, B. Fornberg, D. D. Knight, J. W. McLean, P. G. Saffman, and H. C. Yuen, Calculations of laminar viscous flow over a moving wavy surface, *J. Fluid Mech.* **124**, 347 (1982).
5. J. M. Floryan, Stability of wall bounded shear layers with simulated distributed surface roughness, *J. Fluid Mech.* **335**, 29 (1997).
6. J. M. Floryan and C. Zemach, Schwarz–Christoffel methods for conformal mappings of regions with a periodic boundary, *J. Comput. Appl. Math.* **46**, 72 (1993).
7. J. M. Floryan and U. Dallmann, Flow over a leading edge with distributed roughness, *J. Fluid Mech.* **216**, 629 (1990).
8. J. C. Lin, M. J. Walsh, and R. D. Watson, Turbulent drag characteristics of small amplitude rigid surface waves (AIAA Paper 83-0228), in *21th Aerospace Sciences Meeting, 1983*.
9. J. W. McLean, Computations of turbulent flow over a moving wavy boundary, *Phys. Fluids* **26**, 2065 (1983).
10. J. Rokicki and J. M. Floryan, Higher-order unstructured domain decomposition method, *Comput. Fluids* **28**, 87 (1999).
11. I. J. Sobey, On the flow through furrowed channels. Part 1. Calculated flow patterns, *J. Fluid Mech.* **96**, 1 (1980).
12. J. F. Thompson, Z. U. Warsi, and C. W. Mastin, *Numerical Grid Generation: Foundations and Applications* (North-Holland/Elsevier, New York, 1985).